Lab on a Chip

Accepted Manuscript

This article can be cited before page numbers have been issued, to do this please use: M. Xavier, S. H. Holm, J. P. Beech, D. Spencer, J. O. Tegenfeldt, R. Oreffo and H. Morgan, *Lab Chip*, 2019, DOI: 10.1039/C8LC01154K.

ROYAL SOCIETY OF CHEMISTRY

rsc.li/loc

ROYAL SOCIETY OF CHEMISTRY View Article Online
DOI: 10.1039/C8LC01154K

Lab on a Chip

ARTICLE

Label-free enrichment of primary human skeletal progenitor cells using deterministic lateral displacement

Received 00th January 20xx,
Accepted 00th January 20xx

DOI: 10.1039/x0xx00000x

www.rsc.org/loc

Miguel Xavier,*[a,b] Stefan H. Holm,[c] Jason P. Beech,[c] Daniel Spencer,[a] Jonas O. Tegenfeldt,[c] Richard O. C. Oreffo,[b] and Hywel Morgan[a]

Skeletal stem cells (SSCs) are present in bone marrow (BM) and offer great potential for bone regenerative therapies. However, in the absence of a unique marker, current sorting approaches remain challenging in the quest for simple strategies to deliver SSCs with consistent regeneration and differentiation capacities. Microfluidics offers the possibility to sort cells marker-free, based on intrinsic biophysical properties. Recent studies indicate that SSCs are stiffer than leukocytes and are contained within the larger cell fraction in BM. This paper describes the use of deterministic lateral displacement (DLD) to sort SSCs based on cell size and stiffness. DLD is a technology that uses arrays of micropillars to sort cells based on their diameter. Cell deformation within the device can change the cell size and affect sorting – here evidenced using human cell lines and by fractionation of expanded SSCs. Following sorting, SSCs remained viable and retained their capacity to form clonogenic cultures (CFU-F), indicative of stem cell potential. Additionally, larger BM cells showed enhanced capacity to form CFU-F. These findings support the theory that SSCs are more abundant within the larger BM cell fraction and that DLD, or other size-based approaches, could be used to provide enriched SSC populations with significant implications for stem cell research and translation to the clinic.

1. Introduction

Medical advances have extended life expectancy in developed countries from an average of just 65 years of age in 1950 to almost 80 years of age today.[1] However, this increase in longevity is also associated with exacerbated health issues.[2,3] Thus, within the musculoskeletal arena, increased bone and joint trauma and an increase in a number of metabolic bone diseases has driven the need for efficacious strategies to aid repair and regeneration.

Skeletal stem cells refer specifically to the multipotent, self-renewing stromal cells, which reside in the human bone marrow (BM) with the potential to differentiate and form the skeletal-specific tissues of bone, cartilage and marrow adipocytes.[4,5] While the term mesenchymal stem cells (MSCs; undifferentiated multipotent cells of the mesenchyme), has gained wide acceptance, this term is non-specific and the term skeletal stem cell (SSC) will be used throughout this paper to restrict description to stem cells from bone marrow that are able to generate all skeletal tissues. Applications of SSCs include i) the fundamental study of stem cells, disease mechanisms, and the developmental processes of musculoskeletal tissue, ii) pharmaceutical studies targeting bone and joint disease, and iii) the use of SSCs for regenerative medicine applications in the clinic including stem cell therapies and tissue engineering. The ability of BM stromal cell populations to generate skeletal tissue *in vivo* has repeatedly been demonstrated.[6–12]

However, important challenges remain hampering the routine clinical translation of SSCs, including the development of facile strategies to enrich and generate pure, homogeneous SSC populations from human BM.[5,7] Indeed, one study which used BM progenitors to treat osteonecrosis and fracture non-unions related the success of the procedure with the concentration of progenitors in the bone marrow graft. Critically, the study determined that the concentration needed for the treatment to succeed exceeded the levels present in fresh iliac crest aspirations, emphasising the need for the development of cell enrichment strategies.[13–15]

Typical SSC enrichment methods exploit cell adhesion to tissue culture plastic in the presence of adhesion proteins from foetal calf serum. However, plastic adhesion is non-specific, time-consuming and can result in the alteration of the original SSC phenotype in BM.[16] To enhance the specificity of adhesion isolation protocols, antibody-based fluorescence or magnetic cell sorters (FACS and MACS) are often used. Recent work from Chan and colleagues[17] offers a possible approach to enrich SSCs using judicious selection of negative and positive markers (positive for PDPN, CD73 and CD164 and negative for CD146) but the process remains challenging and advances from antibody-dependent isolation methods are still required.[18–20] In addition, FACS and MACS are costly and involve lengthy protocols that may affect cell viability and hamper their clinical use.[21,22]

[a] Faculty of Physical Sciences and Engineering, and Institute for Life Sciences, University of Southampton, SO17 1BJ, United kingdom.
[b] Centre for Human Development, Stem Cells and Regeneration, Institute of Developmental Sciences, Southampton General Hospital, Tremona Road, SO16 6YD Southampton, United Kingdom.
[c] Division of Solid State Physics and NanoLund, Lund University, SE-221 00, Sweden.
Electronic Supplementary Information (ESI) available. See DOI: 10.1039/x0xx00000x

There is thus an unmet need for new methods that provide facile, cost-effective, homogeneous SSC populations. The development of sorting mechanisms that do not depend on the use of antibodies offers an attractive alternative for delivering cells in an unaltered state. In addition, sample preparation is typically simplified and systems tend to be easier to use.

Microfluidics offers the potential of 'label-free' sorting of particles based on biophysical properties, including size, stiffness, shape and, dielectric and acoustic properties (Xavier *et al.*).[18] Microfluidic cell sorting can be achieved using passive or active approaches, some of which have been directed towards stem or progenitor cell sorting. Active sorting refers to the use of external fields that act on the particles or flow. These include, but are not limited to, i) dielectrophoresis,[23–25] which uses a non-homogeneous electric field to sort cells based on size and membrane capacitance; ii) acoustophoresis, which uses bulk[26,27] or surface[28] ultrasonic waves to sort cells based on differences in size, density and compressibility; and iii) magnetophoresis, which provides sorting based on cells magnetic susceptibility, either intrinsic[29] or aided by superparamagnetic tags.[30,31] Passive sorting exploits hydrodynamic phenomena and microfluidic channel structures to achieve sorting using simple devices and typically at high throughput. Relevant examples include, among others, filtration,[32,33] inertial focusing[34,35] and deterministic lateral displacement (DLD).[29,36]

DLD, first described in 2004 by Huang *et al*.,[37] uses arrays of offset micropillars within a flow channel to sort cells based on diameter, at throughputs of thousands per second. The gap between the pillars and the angle of the pillar array with relation to the main flow direction defines a critical size for separation (*Dc* = critical diameter). Particles smaller than *Dc*, zigzag through the pillar array with no net displacement. In contrast, particles larger than *Dc* are deflected by each pillar and become displaced from their original lateral position at the device inlet (Figure 1, left). To date, DLD has been used to sort multiple particles including beads, bacteria, parasites, circulating tumour cells and blood cells (see McGrath *et al*.).[36] Several variations on the original DLD concept have been reported including sorting particles by physical properties such as shape,[38,39] stiffness/ deformability,[38,40,41] density,[42] and acoustic[43] and dielectric properties.[43,44] Separation by stiffness is based on the fact that two cells of similar size but with significantly different mechanical properties will have different effective radii as they deform due to shear stress and interaction with the micropillars at high flow rates/hydrodynamic pressure (Figure 1, right).

We recently demonstrated that expanded SSCs are stiffer than the three main white blood cell (WBC) populations, present in BM.[45] Furthermore, single cell impedance cytometry measurements indicated that unexpanded SSCs are contained within the larger cell fraction in BM.[16] This paper aims to demonstrate, for the first time, the potential of DLD to achieve microfluidic label-free enrichment of SSCs from primary human BM samples. The difference in stiffness between expanded SSCs and WBCs could be exploited to enhance SSC enrichment from BM by DLD. In addition, the fractionation of human BM cells into size-based sub-populations would enable verification of SSCs in the larger cell fraction, as previously identified by impedance cytometry.[16] Critically, the development of a simple device that would allow enrichment of SSCs without the use of label conjugates (antibodies) could provide cells in an unaltered state with significant implications for their clinical application.

2. Materials and Methods

2.1 Experimental setup

Three different DLD device designs were used with different critical diameters. Design 1 (*Dc* = 17.5 µm) was used to validate the efficiency of DLD as a size-based sorting technique and to demonstrate how cell deformability could affect the outcome of cell sorting using the human osteosarcoma cell line MG-63 as a model. Design 2 (*Dc* = 5.3 µm and 12.2 µm) was used to sort a mixture of two cell lines (MG-63 and HL-60) as a function of cell size and stiffness, with purity quantified by fluorescence flow cytometry. Finally, design 3 (*Dc* = 7.5 µm) was used to enrich human SSCs from primary human BM samples. The mean cell size in each outlet was estimated by flow cytometry, and cell functionality demonstrated by a colony formation assay.

2.2 DLD design considerations

Design 1 is based on the original DLD design of Huang *et al*.[37] and uses sheath flow to hydrodynamically focus the sample in a narrow stream, keeping cells away from the channel walls where sorting efficiency may be affected (Figure 2, top; ESI Figure 1). This provides the highest resolution but leads to significant sample dilution by sheath flow. Given the rarity of SSCs in human BM (< 1 in 10,000-100,000 nucleated cells),[46] a high throughput separation method is critical to enable a practical number of cells to be sorted for clinical application. Accordingly, design 2 uses a single inlet and is sheathless, which leads to higher throughput and allows device operation with a single input (syringe pump or compressed air, see Holm *et al*.[47]). Given the sample is not focused at the inlet, the device has two consecutive sections with different *Dc*. Section 1, with a smaller *Dc*, displaces all particles towards the outer walls using a mirrored micropillar array to create a central cell-free stream. The second section, with a larger *Dc* and inverted microarray direction, displaces only the larger particles back to the centre of the device where they are collected in one of two outlets (Figure 2, middle; ESI Figure 1).

Given human BM contains cells with sizes spanning from only a few microns (red blood cells, small lymphocytes) to over 100 microns (megakaryocytes),[18] sheathless devices to sort primary BM samples must concurrently incorporate a section with a small *Dc* (to displace the smallest cells) and a large gap between micropillars (to avoid clogging), which leads to impractical long devices. Thus, design 3 combines the principles from designs 1 and 2 using sheath flow (in a 1:1 ratio with the sample) and a mirrored micropillar array to achieve separation using one section of a single *Dc* (Figure 2, bottom; ESI Figure 1). In addition, all device designs include a filter array at the device inlets to avoid clogging at the displacement arrays. Further details of the 3 designs can be found in ESI Table 1.

View Article Online
DOI: 10.1039/C8LC01154K

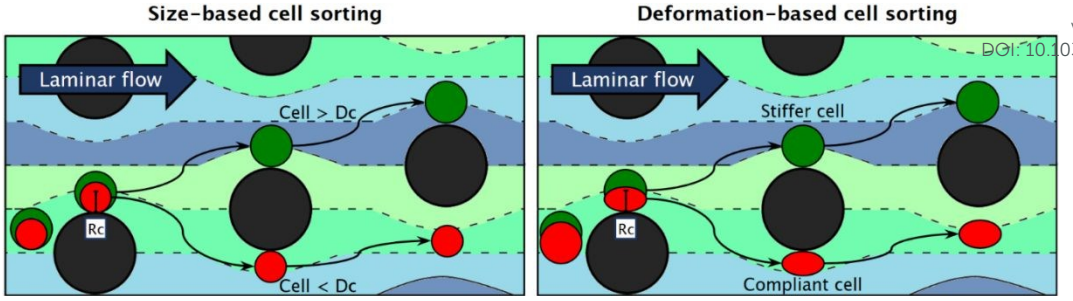

Figure 1 – Particle sorting by deterministic lateral displacement based on differences in particle size (left) and deformation (right). For size-based separation, particles with a radius smaller than *Rc* (*Rc* = *Dc*/2) are predominantly affected by the streamline flowing closest to the micropillar and are not forced to cross streamlines, zigzagging through the microarray. In deformation-based cell sorting, particles with similar size but different deformability are sorted due to an effective change in particle radius by deformation due to gradient shear stresses, acceleration and interaction with the micropillars. Here, the more compliant red particle deforms to an extent that the particle radius becomes smaller than R_C allowing the red particle to continue along the original streamline with no net displacement.

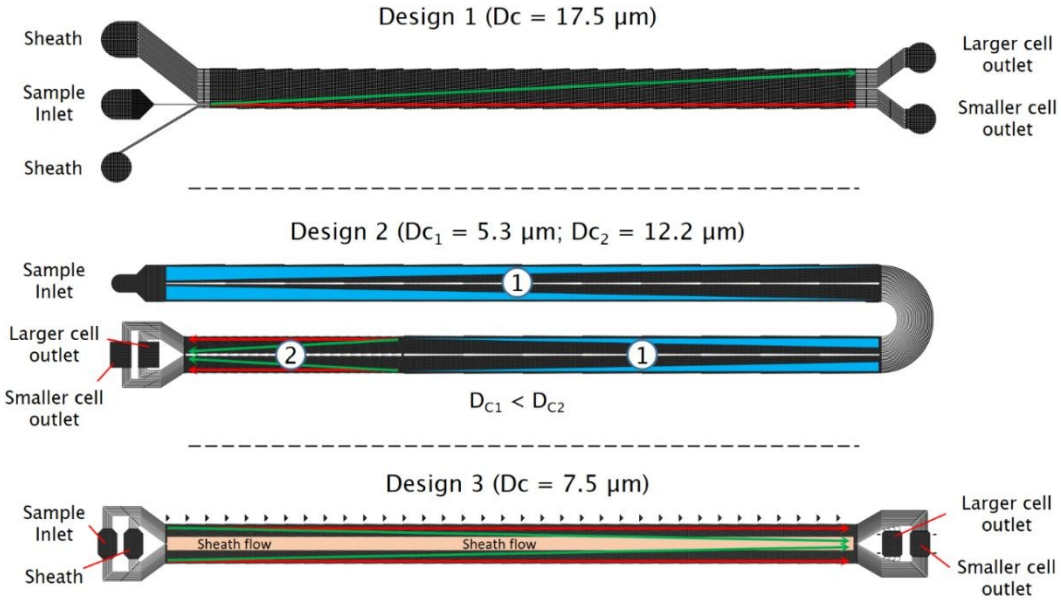

Figure 2 – Diagram of the three different DLD device designs 1-3. In Design 1, particles are initially focused hydrodynamically into a single flow stream. Larger particles (green) are displaced away from the smaller particles (red) which zigzag through the pillar array maintaining a null net displacement. In Design 2, particles introduced from a single inlet are initially displaced towards the outer channel walls in a mirrored section with a small critical separation size (*Dc*), creating a central cell-free stream. In section 2, the direction of the micropillar array is inverted vertically and the *Dc* increased to displace only larger particles (green) into the central cell-free stream while smaller particles (red) continue zigzagging near the channel walls. Design 3 combines the principles used in designs 1 and 2 and uses sheath flow to create the central cell-free stream and a single section with mirrored micropillar array to displace larger particles towards the centre of the device.

2.3 Device design and fabrication

DLD devices were designed using CleWin4 from WieWeb Software (Hengelo, The Netherlands). Important design considerations included the edge correction method proposed by Inglis[48] to minimise wall effects (designs 1-3) and careful calculations and CFD simulations (COMSOL Multiphysics 4.3, Comsol AB, Stockholm, Sweden) to assure that a constant hydraulic resistance was kept across the width of the device wherever different sections were connected by channels of variable length (designs 2-3). More information on both methods can be found in ESI. To avoid clogging in the displacement arrays, a filter array of micropillars with gap size smaller than the gap of the displacement arrays was included at the device inlets. The filters were designed to allow sorting for the duration of a typical experiment, which in this work ranged from around 1 to 3h. The mask designs can be downloaded from the data repository that supports this manuscript.

Photo-lithographic chrome masks in soda lime glass were manufactured by JD Photodata (Herts, UK). Silicon master moulds were fabricated using SU-8 photoresist (SU-8 50 and SU-8 3025, MicroChem Corp., Westborough, MA, USA) following standard techniques, detailed in ESI. Before sorting experiments, the devices were hydrated with a 0.5% (w/v) Pluronic® F-127 solution in PBS to prevent particle adhesion.

2.4 Sample preparation

Polystyrene beads were suspended in a 14 % sucrose (w/v), 0.1% Tween® 20 (v/v) solution in 1x PBS. Cells were suspended in a 15 % (w/v) Ficoll® PM400, 0.5 % (w/v) BSA and 2 mM EDTA solution in 1x PBS. Sucrose and Ficoll® were used to increase the suspending medium density to 1.05 $g \cdot mL^{-1}$ to avoid sedimentation. Tween® 20 was used to prevent bead aggregation and BSA and EDTA were used to prevent cell aggregation and adhesion to the device walls. The sample concentration was kept in the range (0.5 - 2) x 10^6 $cells \cdot mL^{-1}$.

2.5 Device operation

DLD devices were mounted on a portable microscope built in-house to image particle flow and monitor the flow stability (ESI Figure 3). Sample reservoirs were connected to the device using 1.6 mm outer diameter polymer tubing and flow was driven by constant pressure (design 1) or a syringe pump (designs 2 and 3). For design 1, the pressure at the three inlets was controlled using an OB1 MK3 multi-channel flow controller (Elvesys, Paris, France). The devices were primed with suspending buffer for 20 min. before use, and the flow was allowed to stabilise prior to any fraction collection. Where necessary, to guarantee sample sterility, tubing and fittings were autoclaved and the DLD devices were exposed to UV light for 20 min., primed with 70 % ethanol for 20 min. and the experiments run in a laminar flow hood.

The purity at each outlet was defined as the relative fractions of each particle type among the particles of interest in the respective outlet. Note that this means that the purity is dependent on the mixing ratio at the inlet (Figures 3, 5 and 7). When just one cell population was fractionated, the sorting efficiency was defined as the fraction of that population that collected at each outlet (Figures 3, 6 and 8).

2.6 Cell culture

Cells were maintained in media supplemented with 10 % foetal calf serum (FCS) and 100 $U \cdot mL^{-1}$ penicillin and 100 $\mu g \cdot mL^{-1}$ streptomycin (1 % Pen/Strep). This is referred to as complete media. Otherwise, it is indicated as plain media. Cells were maintained in a humidified chamber at 37 ℃ and 5 % CO_2. To detach adherent cells, a trypsin-EDTA solution (0.5 $g \cdot L^{-1}$ trypsin; 0.2 $g \cdot L^{-1}$ EDTA) was used for 5-10 min. Given SSCs produce significant amounts of extra-cellular matrix, following expansion, adherent SSCs were pre-treated with collagenase IV (200 $\mu g \cdot ml^{-1}$) in plain α-MEM for 40 min. This reduced the amount of debris and cell aggregates that could block the DLD devices. Details of the culture conditions of the MG-63, GFP^+ MG-63 and HL-60 cells lines can be found in ESI.

Given that this manuscript focuses on size-based cell sorting, Table 1 shows the mean diameter of the cell populations used in this study. Mean cell sizes were estimated using microfluidic impedance cytometry, reported elsewhere.[16]

Table 1 – Mean and composite standard deviation of the size measurements (cell diameter) obtained by single cell impedance cytometry[16] of the cell populations used in this study. The values for BMSCs and SSCs P0 refer to Stro-1^+/$CD146^+$ cells from primary human BM and to Stro-1^+ SSCs following 2-week expansion in tissue culture plastic respectively. The size ranges indicated for lymphocytes and granulocytes were obtained from the literature.[49–51]

	BMSCs	SSCs P0	HL-60	MG-63	Lymphocyte	Granulocyte
Mean ± STD (μm)	9.1 ± 1.6	18.2 ± 3.1	11.4 ± 1.4	19.5 ± 2.4	6 - 9 μm	12 - 15 μm

2.6.1 Isolation of primary human bone marrow mononuclear cells (BMMNCs). Human BM samples were obtained from patients undergoing total hip replacement surgeries at the Spire Southampton Hospital or the Southampton General Hospital, with full patient consent. Only tissue that would have been discarded was used, with approval of the Southampton and South West Hampshire Research Ethics Committee (Ref no. 194/99/1 & 210/01). Following cell extraction from BM, the samples were washed with plain α-MEM and the cell suspension filtered through a 70-μm cell strainer and layered upon Lymphoprep™ to remove red blood cells (RBCs) and the majority of granulocytes by density centrifugation. The BMMNC fraction was collected from the 'buffy coat', washed by centrifugation and re-suspended to yield the population of 'unsorted' human BMMNCs. For MACS sorting of Stro-1^+ cells, BMMNCs were incubated with the Stro-1 monoclonal antibody (IgM) from mouse hybridoma produced *in loco* and the Stro-1^+ cell population was isolated by magnetic separation of cells labelled with anti-mouse IgM microbeads, as previously detailed.[52,53] The enriched Stro-1^+ population was plated and the adhered fraction is referred to as SSCs passage 0 (P0).

2.6.2 Human blood samples. Ethical approval was given by the Isle of Wight, Portsmouth and South East Hampshire Local Research Ethics Committee (Ref no. 06/Q1701/137) and written consent was obtained from all participants for sample collection. Blood samples were collected from healthy volunteers through a finger prick using a safety lancet into collection tubes coated with sodium citrate to prevent the coagulation cascade. The tubes were kept on a roller at room temperature and subsequent experimental work was carried out within 2 to 3 hours after collection. RBC lysis was achieved by addition of a lysis solution (0.12 % (v/v) formic acid, 0.05 % saponin (w/v) in distilled water) in a 12:1 ratio (lysis solution : whole blood). After constant mixing for 6 seconds the reaction was halted by the addition of 5.3 μL of an isosmotic quencher (0.6 % w/v sodium carbonate, 3 % w/v sodium chloride solution in distilled water) per microliter of whole blood. White blood cells (WBCs) were spun down, re-suspended and mixed for sorting in the intended ratio.

2.7 Flow Cytometry

Protocols for fluorescent cell staining can be found in ESI. Cells and particles were suspended in running buffer, filtered through a 100-μm cell strainer and analysed using a BD® Accuri C6 or a BD® FACSCanto flow cytometer (Becton, Dickinson and Company, Franklin Lakes, NJ, USA). Data analysis was performed using FlowJo V10 software (FlowJo LLC, Ashland, OR, USA). Single events were gated for linearity in the forward scatter (FSC-H *vs* FSC-A) plot and typically, 20,000 events were acquired for each measurement. Events were considered fluorescently positive above the threshold at which fewer than 1 % were positive for the matched isotype control.

2.8 CFU-F staining and counting

SSCs, cultured in 6-well plates for 2 weeks, were washed with PBS and fixed with 95 % (v/v) ethanol in dH_2O for 10-15 minutes. Fixed cultures were incubated with a 0.05 % crystal violet solution in dH_2O for 5 minutes and washed extensively before

imaging. Stained colonies (50+ cells) were counted and imaged using a dissecting stereoscope.

2.9 Statistical analyses

Results are displayed as Mean ± SD, unless otherwise stated, using GraphPad Prism 7 (San Diego, CA, USA). Data distributions were tested for normality using the Shapiro-Wilk test. The statistical significance was tested using the Student's t-test for independent samples, or a one-way analysis of variance (ANOVA) with Tukey's post-hoc test, for sample variables that followed a normal distribution. Sample variables that did not follow a normal distribution were tested using a Kruskal-Wallis test followed by a Mann Whitney-U (IBM SPSS Statistics® v24, Armonk, NY, US). The standardised Z-score was used to calculate the percentage of a particle population (which size follows a normal distribution with known mean and standard deviation), that fell under the *Dc* of a DLD device 1. The standardised Z-score was calculated using equation 1 (where μ and σ are the mean and standard deviation respectively) and percentages according to the calculated Z-score were obtained from the normal distribution table (ESI Tables 4 and 5).

$$Z = \frac{x - \mu}{\sigma} \quad (\textbf{Equation 1})$$

3. Results and Discussion

3.1 Device 1

3.1.1 Non-deformable polystyrene beads. To determine the efficiency of Device 1 (*Dc* = 17.5 μm), 16 μm (15.66 ± 1.43, Mean ± SD) and 24 μm (23.74 ± 1.41) non-deformable polystyrene beads were mixed 1:1 and flowed through the device. It should be noted that considering the mean size and standard deviation of the particles, the size distribution of the 16-μm beads partially overlaps with the device *Dc*. Assuming the bead diameter is normally distributed, it is possible to estimate the fraction of beads that are larger than 17.5 μm using the standardised Z-score (equation 1). According to the normal distribution table (ESI Tables 4 and 5), around 10.2 % of the 16-μm beads should be larger than 17.5 μm and appear in the larger-cell outlet.

The bead suspension was pumped through the device at 10,000 beads·min^{-1} at an inlet pressure of 250 mbar. The separation efficiency was quantified by analysing the fractions collected at each outlet by flow cytometry (Figure 3a). The larger and smaller bead outlets had purities of 88.5 ± 7.6 % and 98.3 ± 2.1 % respectively (N=6). This was in line with the predicted percentages (given the standard deviation of the 16-μm particles) and showed that DLD offered the potential of label-free sorting with high purity, which for the smaller beads was typically over 99% (for 4 out of the 6 measurements) and as high as 99.8 %.

For non-deformable particles, sorting should be independent of flow rate. To demonstrate this, the same bead mixture was separated at increasing inlet pressures (100-1,000 mbar). Figure 3b shows the purity of the smaller beads (closed circles) and larger beads (open circles), which remained constant throughout the range of input pressures even up to 1 bar. This experiment was only conducted once and intra-experimental variability explains the minor inconsistency of the purity values for different input pressures.

3.1.2 Binary fractionation of MG-63 as a function of cell deformability. To demonstrate that cell deformation affects the outcome of cell sorting by DLD, a human osteosarcoma cell line (MG-63) was pumped through Device 1 at pressures between 100 to 1,000 mbar. These cells have a diameter of 19.5 ± 2.4 μm,[16] so it was expected that at lower flow rates (low deformation), the majority of MG-63 would be displaced and appear at the larger-cell outlet. Figure 3b shows that at 100 mbar, more than 65 % of the MG-63 cells were displaced by the micropillar array and exited at the larger-cell outlet (blue dotted bar, N=2). Higher input pressures increased the flow rates and shear stresses, leading to pronounced cell deformation. This reduces the apparent size of the MG-63 and the fraction of cells displaced fell to under 20 % at 1,000 mbar. Note that same pressure did not alter the purity of sorted 16 μm and 24 μm polystyrene beads. Figure 4 shows sequential images of a single MG-63 cell deforming upon interaction with a DLD micropillar at 1,000 mbar. As the cell is deformed (Figure 4 b-d), the cell radius becomes smaller than *Dc* so that it zigzags past the micropillars (Figure 4 e-f).

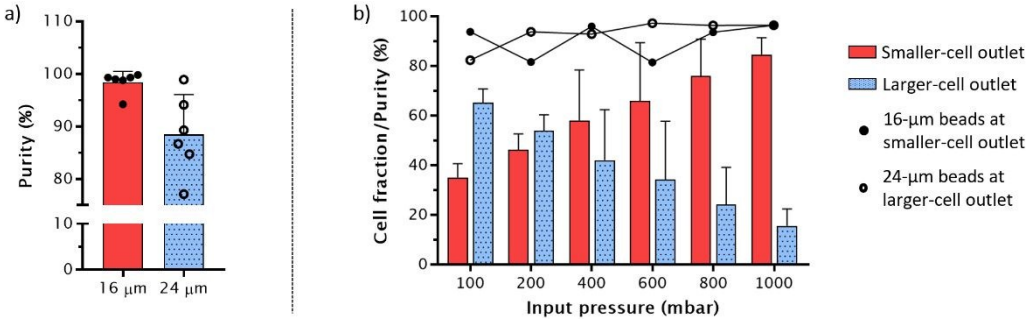

Figure 3 – a) Purity of 16 μm (red) and 24 μm (blue, dotted) diameter beads mixed 1:1 and sorted at an inlet pressure of 250 mbar. Graph bars show mean ± SD (N=6) and circles show the mean purity of individual experiments. b) Binary fractionation of MG-63 as a function of cell deformation after increasing overpressure at the inlet (100-1000 mbar). Blue (dotted) and red bars show the percentage of MG-63 collected at the larger-cell and smaller-cell outlets respectively (N=2). Higher flow rates led to accentuated cell deformation. As a control, non-deformable 16 μm (closed circles) and 24 μm (open circles) diameter polystyrene beads were sorted at the same flow rates with the purity remaining constant up to 1 bar.

View Article Online
DOI: 10.1039/C8LC01154K

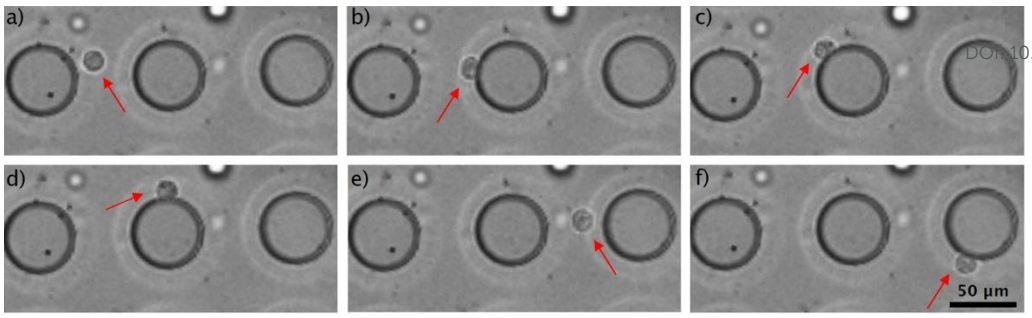

Figure 4 – Cell deformation in a DLD device. a) to f) are images of a single MG-63 (red arrow) cell flowing from left to right through a DLD micropillar array at an inlet pressure of 1,000 mbar (corresponding to a speed of 10 cm·s^{-1}). Images were taken using a high-speed camera (Vision Research, Wayne, NJ, USA) and bespoke software (Phantom Camera Control Software, Vision Research). Cell deformation changes the effective cell size altering its trajectory in the DLD device.

3.2 Device 2

3.2.1 Size and mechano-based sorting of MG-63 and HL-60. To assess whether cell deformation could improve the purity of mixed cell populations sorted by DLD, MG-63 and HL-60 cells were mixed 1:1 and sorted using Device 2 (*Dc* = 12.2 µm). To facilitate cell discrimination, GFP$^+$ MG-63 were used together with CellTracker™ (deep red) labelled HL-60 cells. The size of the HL-60 is smaller than the MG-63, at 11.4 ± 1.4 µm.[16] Mechanical phenotyping studies also showed that MG-63 are significantly stiffer than HL-60, with a Young's modulus approximately two-fold higher.[45] Given the large difference in size between the two cell types, a high sorting purity could be anticipated. The purity of HL-60 and MG-63 (measured by flow cytometry) in the smaller-cell and larger-cell outlet respectively was in excess of 90 % at a flow rate of 15 µL·min^{-1} (Figure 5a-b). Fluorescence microscopy images validated the separation obtained (ESI Figure 4).

Higher flow rates led to increased cell deformation and at 30 µL·min^{-1} the deformation of HL-60 meant that fewer HL-60 cells were present in the larger-cell outlet, increasing the purity of MG-63 cells in this outlet to 98 % (Figure 5b). Increasing the flow rate to 200 µL·min^{-1} did not further increase the purity of MG-63 significantly, suggesting that the HL-60 cells could not be deformed further. In contrast, the more deformable MG-63 cells continued to change as the flow rate increased from 15 to 200 µL·min^{-1}. This led to an increase in the number of MG-63 cells collected in the smaller-cell outlet at higher flow rates (Figure 5a) indicating that cell deformation changes the effective size of MG-63 cells below the device *Dc*.

3.2.2 Binary fractionation of SSCs as a function of cell deformability. Deformation-based DLD sorting was used to determine whether large or small diameter SSC fractions displayed distinct clonogenic potential. Stro-1$^+$ MACS-sorted human SSCs were expanded for 2 weeks, harvested and sorted into two fractions of different sizes using device 2 (*Dc* = 12.2 µm) at flow rates varying from 15 to 100 µL·min^{-1}. After sorting, 100 cells from each fraction were plated into 6-well plates in triplicate to assess their capacity to form colony-forming units-fibroblastic (CFU-F).

At 15 µL·min^{-1} the majority of SSCs (95 %) collected at the larger-cell outlet (Figure 6a). This was expected given the mean size of expanded SSCs at passage 0 (P0), estimated at 18.1 ± 3.1 µm.[16] With increasing flow rate, a higher fraction of SSCs collected at the smaller-cell outlet (~ 25 % at 100 µL·min^{-1}). This indicated that cell deformation affected the SSCs sufficiently to alter their sorting outcome.

The mean size of SSCs collected at each outlet, estimated by flow cytometry from the forward scatter signal (FSC-A), was statistically different at all flow rates tested (Figure 6b). As the flow rate increased, SSC deformation led to an increase in the mean cell size of cells collected in the smaller-cell outlet because of larger cells flowing in zigzag mode. The contour plots, obtained by flow cytometry, of the cell populations collected at both outlets are shown in ESI Figure 5. The capacity to form CFU-F was not significantly affected by DLD, when compared to unsorted SSCs (Figure 6c), confirming that exposure to shear in DLD did not affect basic cell function, even at the highest flow rate (100 µL·min^{-1} or >4 cm·s^{-1}). These results support previous studies that demonstrated no significant reduction in the cell viability of 3 cancer cell lines sorted by DLD at 10 mL·min^{-1}, or a maximum velocity of 150 cm·s^{-1}.[54] Another study from Di Carlo's group showed no significant differences in cell viability and gene expression of MCF7 cells exposed to high shear in an inertial microfluidics device.[55] Thus, shear-induced cell-death appears not to be a limitation in the operation of DLD devices.

Cells collected at both smaller-cell and larger-cell outlets displayed equivalent CFU-F formation capacity, when sorted at 30, 50 and 100 µL·min^{-1}. Interestingly, at 15 µL·min^{-1}, where the largest difference in the mean cell size was observed, cells collected at the larger-cell outlet displayed greater CFU-F formation (Figure 6c). The difference observed was not statistically significant (p=0.18, N=3) but is denoted in the images shown in ESI Figure 6. This suggested that larger SSCs may have a higher capacity to form clonal populations – indicative of the self-renewal capacity associated with stem cells. This was in keeping with previous observations by Poon[35] and Yin[34] *et al.* who also found a correlation between the size of MSCs, sorted using an inertial microfluidics approach, and their multipotency; osteogenic and chondrogenic potential; and the capacity to promote BM regeneration *in vivo* – all of which are fundamental differentiation potentialities credited to SSCs.

View Article Online
DOI: 10.1039/C8LC01154K

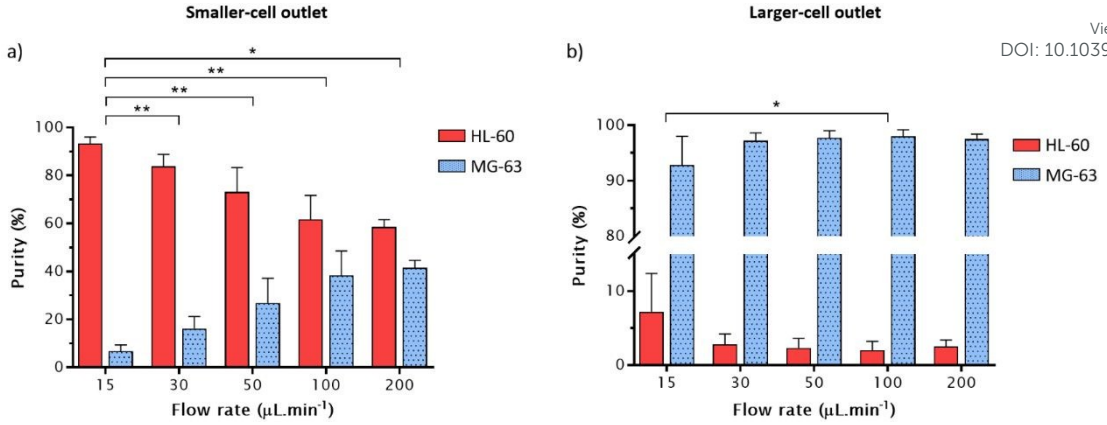

Figure 5 – Purity of MG-63 (blue, dotted) and HL-60 (red) cells collected from the smaller-cell (a) and larger-cell (b) outlets, after separation at varying flow rates (15-200 µL·min-1). Values show mean ± SD (N=5; N=4 for flow rate 200 µL·min-1; *p < 0.05; **p < 0.01 with p-values obtained using a one-way analysis of variance (ANOVA) with Tukey's post-hoc test for sample variables that followed a normal distribution (smaller-cell outlet) or a Kruskal-Wallis test followed by a Mann Whitney-U otherwise).

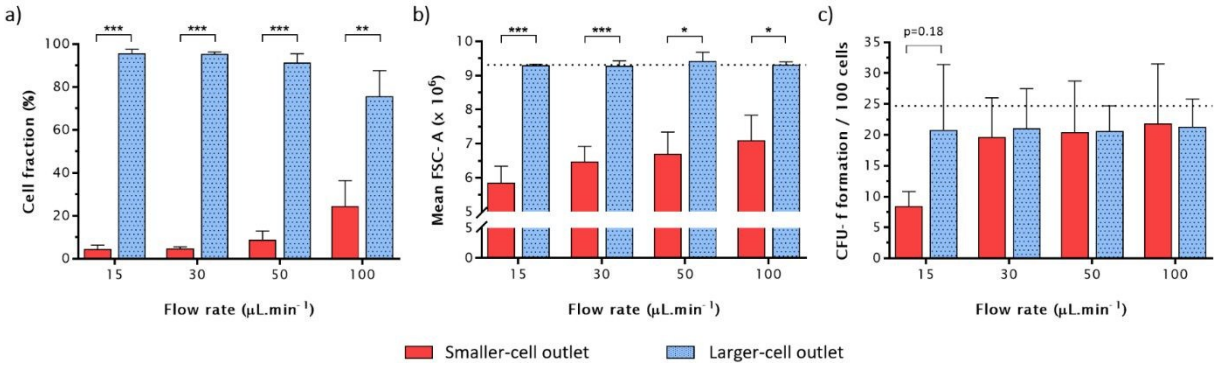

Figure 6 – Fraction of SSCs collected at the smaller-cell (red) and larger-cell (blue, dotted) outlets *vs* flow rate. b) Mean FSC-A values of the cells collected at the smaller-cell (red) and larger-cell (blue, dotted) outlets, respectively. d) CFU-F formation capacity of SSCs after sorting by DLD for the two outlets. Overall, the capacity to form CFU-F was not affected by DLD (dashed line shows the number of CFU-F obtained from unsorted SSCs). At 15 µL·min-1, where the highest difference in cell size was observed, larger cells (blue, dotted) displayed a higher capacity to form clonogenic cultures when compared with SSCs collected in the smaller-cell outlet (red). Values show mean ± SD (N=3; *p < 0.05; ***p < 0.001 with p-values obtained using the Student's t-test for independent samples).

3.2.3 Size and mechano-based sorting of SSCs and WBCs. Device 2 used a sheathless design to achieve sorting by DLD at higher throughput. The *Dc* of section 1 was set at 5.3 µm to displace the different cell populations present in human BM, which include WBCs, and create a central cell-free stream. To test this concept, expanded SSCs at P0 were sorted from WBCs obtained from healthy volunteers. Briefly, WBCs were fluorescently labelled with a fluorescent CD45 label (allophycocyanin, APC) and mixed 2:1 with SSCs (tagged with CellTracker™ green, CTG). Data from a single experiment showed the anticipated high purity of WBCs in the smaller-cell outlet, which reached 99.6 % at 15 µL·min^{-1} and decreased to 95.3 % at 100 µL·min^{-1} due to deformation of the SSCs (Figure 7). Unexpectedly, the purity of SSCs in the larger-cell outlet was only 73 % (at 15 µL·min^{-1}) and decreased at higher flow rates. This was probably due to deformation of WBCs to diameters below the *Dc* of section 1 – 5.3 µm (see supporting data in ESI Figure 7).

These preliminary data indicate that a sheathless DLD device is not the most efficient way of sorting SSC from human BM and provided information for the design of device 3. This device used sheath flow to create a central cell-free stream towards which larger/stiffer cells were sorted.

3.3 Device 3

3.3.1 Enrichment of human primary skeletal progenitor cells. Primary human BM mononuclear cells (BMMNCs), obtained from the buffy coat of human BM samples, were suspended at a concentration of 1-2 x 10^6 cells·mL^{-1} and sorted using device 3 (*Dc* = 7.5 µm) at varying flow rates. At 15 µL·min^{-1} the throughput was 250 cells·s^{-1}, increasing linearly to 850 cells·s^{-1} at 50 µL·min^{-1}. As anticipated, increasing flow rates led to higher ratios of cells collecting in the smaller-cell outlet due to deformation (Figure 8a). The largest difference in the mean cell size of cells at each outlet was observed at 15 µL·min^{-1} (Figure 8b). After sorting, 100,000 cells from each of the sorted fractions were plated into the wells of 6-well plates in triplicate and allowed to adhere and expand to assess their capacity to form CFU-F. BMMNCs collected at the larger-cell outlet showed a higher CFU-F formation capacity at all flow rates examined (statistically significant at 30 µL·min^{-1} due to smaller experimental variation; Figure 8c). These results are in line with cell volume estimates obtained by microfluidic impedance cytometry showing that the SSCs are larger on average than the BMMNC population.[16] Note that at 30 µL·min^{-1} the sorted cells were 50:50 between the two outlets (Figure 8a). Representative images of the CFU-F can be found in ESI Figure 8.

View Article Online
DOI: 10.1039/C8LC01154K

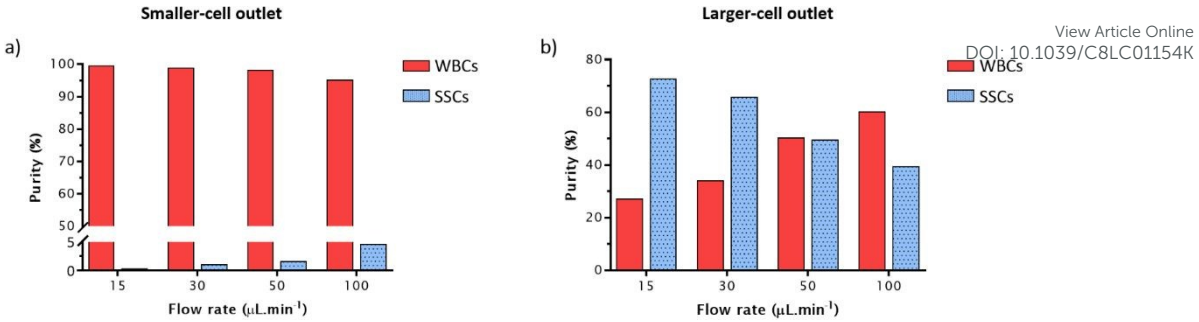

Figure 7 – Purity of SSCs (blue, dotted) and WBCs (red) collected from the smaller-cell (a) and larger-cell (b) outlets after sorting at varying flow rates (15-100 µL·min^{-1}).

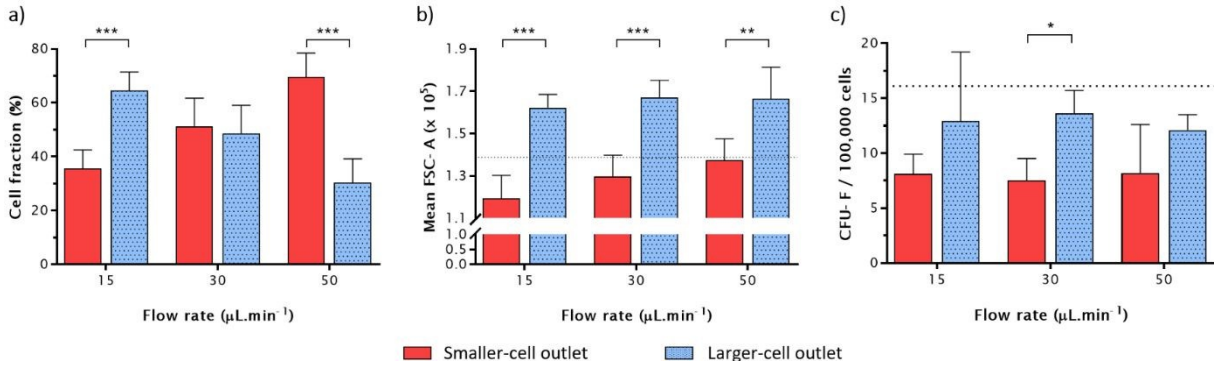

Figure 8 – a) Fraction of human BM mononuclear cells collected at the smaller-cell (red) and larger-cell (blue, dotted) outlets *vs* flow rate. b) Mean FSC-A values of the cells collected at the smaller-cell (red) and larger-cell (blue, dotted) outlets, respectively. Dashed line shows the mean size of unsorted cells. c) CFU-F formation capacity of human BMMNCs after sorting by DLD. At 30 µL·min^{-1}, the number of CFU-F formed from larger SSCs (blue, dotted) was significantly higher (*p < 0.05) than from smaller SSCs (red). Values show mean ± SD (a, b: N=6; c: N=3; *p < 0.05; **p < 0.01; ***p < 0.001 with p-values obtained using the Student's t-test for independent samples).

However, the capacity of unsorted BMMNCs (Figure 8c, dashed line) to form CFU-F was higher than sorted BMMNCs from either outlet. Although sorting by DLD did not affect cell function, we hypothesise that the current protocol leaves cells in nutrient-free buffer for too long (in excess of 2h to sort 2 million cells at 15 µL·min^{-1}). Further improvements include optimisation of the sorting buffer and device parallelisation to increase sorting throughput and critically shorten the sorting time. For example, DLD sorting of circulating tumour cells (CTCs) uses 128 parallel devices to achieve a throughput of 15-20 million cells per second.[56] At a similar throughput, a typical human BM buffy coat could be sorted under a minute, or slightly over considering the transition time of the cells from the entry to the exit reservoirs.

Given the potential application of enriched skeletal progenitor cells in regenerative medicine, including stem cell therapies and tissue engineering, cell recovery post-sorting is of utmost importance. Here, cell recovery was maximised by using a density-matched buffer, which also contained EDTA and BSA to avoid cell aggregation and adhesion to the DLD devices. In addition, the devices were pre-treated with a solution of Pluronic F-127 to further avoid cell adhesion to PDMS. Although the quantification of cell recovery was not the object of this study, cell counts of the fractions collected at both outlets from device 3, showed that cell recovery was significantly higher than 50 %. The latest studies of CTC sorting by DLD showed recovery of 99.5 % of CTCs diluted in whole blood at ratios below 1 in every 1,000,000 cells.[56] Thus, cell recovery in DLD cell sorting of human skeletal progenitor cells is not anticipated to be a significant issue.

While the current design and protocol did not provide the anticipated enrichment, the verification that larger cells show an almost two-fold increase in CFU-F formation capacity validates the finding that SSCs fall within the larger cell population in human BM.[16] This illustrates the potential to design an optimised size-based sorting device, with higher throughput and an improved sorting buffer to provide enriched populations of SSCs sorted by DLD. DLD devices are easy to use and can potentially provide cells in an unaltered state – critical for clinical application. With improved efficiency this technique could deliver BM progenitors at the concentration needed for successful BM grafts with significant clinical impact.[14]

4. Conclusions

This work has demonstrated sorting by DLD based on cell size and deformability using human nucleated cells of different origins. The purity of the MG-63 cells after sorting from a mixture with HL-60 increased from ~90 % to 98 % at flow rates higher than 30 µL·min^{-1}, where cell deformation became important. Expanded SSCs deformed in flow with more cells collecting in the smaller-cell outlet as the flow rate increased. Cells were recovered and cultured under sterile conditions after sorting by DLD and the capacity of sorted SSCs to form CFU-F (indicative of their stem cell potential) was not affected even at the highest flow rate (100 µL·min^{-1}). Where the largest difference in the mean cell size of cells collected in the smaller-

cell and larger-cell outlets was achieved, larger SSCs appeared to have a higher capacity to form CFU-F, consistent with previous observations.[35] A similar trend was observed for BMMNCs after sorting; the larger BMMNCs formed greater numbers of CFU-F than smaller cells at all flow rates. This was in keeping with previous work that showed that SSCs were predominantly located within the larger cell fraction in BM. Although the current designs and experimental protocol require improvement, this study shows the potential of DLD to enrich BM progenitor cells to the levels required for clinical application in regenerative medicine and tissue engineering. Future work might include i) optimising the *Dc* and flow rates ii) optimising the sorting buffer to enhance cell viability and iii) increasing throughput by parallelisation to significantly reduce sorting time.

Data accessibility

The datasets supporting this article are included in the main paper and have been uploaded as part of the electronic supplementary material. Additional datasets are available from https://doi.org/10.5258/SOTON/D0694.

Author contributions

MX designed the DLD devices, fabricated the silicon masters and PDMS devices, carried out all cell culture and biochemical lab work, data processing and statistical analyses, participated in the design of the study, and drafted the manuscript. SHH and JPB contributed to the device designs and performed simulations in COMSOL to pre-assess the device performance. DS participated in the design of the study. JOT, RO and HM designed and coordinated the study. All authors helped draft the manuscript and gave final approval for publication.

Conflicts of interest

There are no conflicts to declare.

Acknowledgements

The authors would like to express their gratitude to the surgeons from the Spire Southampton Hospital and the Southampton General Hospital for providing the patient bone marrow samples and to Dr. Andy Chase from the Wessex Regional Genetics Laboratory for providing the HL-60 cells. The authors would also like to thank Maaike Jongen and Jonathan West for assisting with the high-speed camera videos.

This study was funded by the European Commission through the Label-free particle sorting (LAPASO) ITN project of the European Union's Seventh Framework Programme FP7/2007-2013 under REA grant agreement no. 607350 and by the Institute for Life Sciences, University of Southampton through a Higher Education Innovation Fund (HEIF) allocated to the University by the Higher Education Funding Council for England (HEFCE). SHH, JPB and JOT acknowledge funding from the Swedish Research Council (VR) grant no. 2015-05426.

References

1 United Nations World Population Prospects: The 2015 Revision. (2015).
2 Christensen, K., Doblhammer, G., Rau, R., & Vaupel, J. W. Ageing populations: the challenges ahead. *Lancet* **374,** 1196–1208 (2009).
3 Rachner, T. D., Khosla, S., & Hofbauer, L. C. Osteoporosis: Now and the future. *Lancet* **377,** 1276–1287 (2011).
4 Bianco, P., & Robey, P. G. Skeletal stem cells. *Development* **142,** (2015).
5 Bianco, P. Stem cells and bone: a historical perspective. *Bone* **70,** 2–9 (2015).
6 Bianco, P., Robey, P. G., & Simmons, P. J. Mesenchymal stem cells: revisiting history, concepts, and assays. *Cell Stem Cell* **2,** 313–9 (2008).
7 Gothard, D., Tare, R. S., Mitchell, P. D., Dawson, J. I., & Oreffo, R. O. C. In search of the skeletal stem cell: isolation and separation strategies at the macro/micro scale for skeletal regeneration. *Lab Chip* **11,** 1206–1220 (2011).
8 Quarto, R., Mastrogiacomo, M., Cancedda, R., Kutepov, S. M., Mukhachev, V., Lavroukov, A., Kon, E., & Marcacci, M. Repair of Large Bone Defects with the Use of Autologous Bone Marrow Stromal Cells. *N. Engl. J. Med.* **344,** 385–386 (2001).
9 Petite, H., Viateau, V., Bensaïd, W., Meunier, A., De Pollak, C., Bourguignon, M., Oudina, K., Sedel, L., & Guillemin, G. Tissue-engineered bone regeneration. *Nat. Biotechnol.* **18,** 959–963 (2000).
10 Bianco, P. Stem cells and bone: A historical perspective. *Bone* **70,** 2–9 (2015).
11 Tilley, S., Bolland, B. J., Partridge, K., New, A. M., Latham, J. M., Dunlop, D. G., & Oreffo, R. O. Taking tissue-engineering principles into theater: augmentation of impacted allograft with human bone marrow stromal cells. *Regen. Med.* **1,** 685–692 (2006).
12 Aarvold, A., Smith, J. O., Tayton, E. R., Jones, A. M. H., Dawson, J. I., Lanham, S., Briscoe, A., Dunlop, D. G., & Oreffo, R. O. C. From bench to clinic and back: skeletal stem cells and impaction bone grafting for regeneration of bone defects. *J. Tissue Eng. Regen. Med.* **8,** 779–786 (2014).
13 Tare, R. S., Kanczler, J., Aarvold, A., Jones, M. H., Dunlop, D. G., & Oreffo, R. O. C. Skeletal stem cells and bone regeneration: translational strategies from bench to clinic. *Proc. Inst. Mech. Eng. H.* **224,** 1455–1470 (2010).
14 Hernigou, P., Poignard, A., Beaujean, F., & Rouard, A. H. Percutaneous Autologous Bone-Marrow Grafting for Nonunions: Influence of the Number and Concentration of Progenitor Cells. *J. None Jt. Surg.* (2005).
15 Hernigou, P., Poignard, A., Zilber, S., & Rouard, H. Cell therapy of hip osteonecrosis with autologous bone marrow grafting. *Indian J. Orthop.* **43,** 40–5 (2009).
16 Xavier, M., de Andrés, M. C., Spencer, D., Oreffo, R. O. C., & Morgan, H. Size and Dielectric Properties of Skeletal Stem Cells Change Critically After Enrichment and Expansion from Human Bone Marrow: Consequences for Microfluidic Cell Sorting. *J. R. Soc. Interface* **14,** 20170233 (2017).
17 Chan, C. K. F., Gulati, G. S., Sinha, R. *et al.* Identification of the Human Skeletal Stem Cell. *Cell* **175,** 43–56.e21 (2018).
18 Xavier, M., Oreffo, R. O. C., & Morgan, H. Skeletal stem cell isolation: A review on the state-of-the-art microfluidic label-free sorting techniques. *Biotechnol. Adv.* **34,** 908–923 (2016).
19 Tare, R. S., Babister, J. C., Kanczler, J., & Oreffo, R. O. C. Skeletal stem cells: Phenotype, biology and environmental

niches informing tissue regeneration. *Mol. Cell. Endocrinol.* **288,** 11–21 (2008).
20 Zannettino, A. C. W., Paton, S., Kortesidis, A., Khor, F., Itescu, S., & Gronthos, S. Human mulipotential mesenchymal/stromal stem cells are derived from a discrete subpopulation of STRO-1bright/CD34/CD45(-)/glycophorin-A-bone marrow cells. *Haematologica* **92,** 1707–8 (2007).
21 Grützkau, A., & Radbruch, A. Small but mighty: How the MACS®-technology based on nanosized superparamagnetic particles has helped to analyze the immune system within the last 20 years. *Cytom. Part A* **77A,** 643–647 (2010).
22 Basu, S., Campbell, H. M., Dittel, B. N., & Ray, A. Purification of Specific Cell Population by Fluorescence Activated Cell Sorting (FACS). *J. Vis. Exp* 15463791–1546 (2010). doi:10.3791/1546
23 Vykoukal, J., Vykoukal, D. M., Freyberg, S., Alt, U., & Gascoyne, P. R. C. Enrichment of putative stem cells from adipose tissue using dielectrophoretic field-flow fractionation. *Lab Chip* **8,** 1386–1393 (2008).
24 Song, H., Rosano, J. M., Wang, Y., Garson, C. J., Prabhakarpandian, B., Pant, K., Klarmann, G. J., Perantoni, A., Alvarez, L. M., & Lai, E. Continuous-flow sorting of stem cells and differentiation products based on dielectrophoresis. *Lab Chip* **15,** 1320–1328 (2015).
25 Adams, T. N. G., Jiang, A. Y. L., Vyas, P. D., & Flanagan, L. A. Separation of neural stem cells by whole cell membrane capacitance using dielectrophoresis. *Methods* **133,** 91–103 (2018).
26 Dykes, J., Lenshof, A., Åstrand-Grundström, I. B., Laurell, T., & Scheding, S. Efficient removal of platelets from peripheral blood progenitor cell products using a novel micro-chip based acoustophoretic platform. *PLoS One* **6,** (2011).
27 Lenshof, A., Jamal, A., Dykes, J., Urbansky, A., Astrand-Grundstrom, I., Laurell, T., & Scheding, S. Efficient purification of CD4+ lymphocytes from peripheral blood progenitor cell products using affinity bead acoustophoresis. *Cytom. Part A* **85,** 933–941 (2014).
28 Nawaz, A. A., Chen, Y., Nama, N., Nissly, R. H., Ren, L., Ozcelik, A., Wang, L., McCoy, J. P., Levine, S. J., & Huang, T. J. Acoustofluidic Fluorescence Activated Cell Sorter. *Anal. Chem.* **87,** 12051–12058 (2015).
29 Huang, R., Barber, T. A., Schmidt, M. A., Tompkins, R. G., Toner, M., Bianchi, D. W., Kapur, R., & Flejter, W. L. A microfluidics approach for the isolation of nucleated red blood cells (NRBCs) from the peripheral blood of pregnant women. *Prenat. Diagn.* **28,** 892–899 (2008).
30 Karabacak, N. M., Spuhler, P. S., Fachin, F. *et al.* Microfluidic, marker-free isolation of circulating tumor cells from blood samples. *Nat. Protoc.* **9,** 694–710 (2014).
31 Jing, Y., Moore, L. R., Schneider, T., Williams, P. S., Chalmers, J. J., Farag, S. S., Bolwell, B., & Zborowski, M. Negative selection of hematopoietic progenitor cells by continuous magnetophoresis. *Exp. Hematol.* **35,** 662–672 (2007).
32 McFaul, S. M., Lin, B. K., & Ma, H. Cell separation based on size and deformability using microfluidic funnel ratchets. *Lab Chip* **12,** 2369 (2012).
33 Wang, G., Mao, W., Byler, R., Patel, K., Henegar, C., Alexeev, A., & Sulchek, T. Stiffness Dependent Separation of Cells in a Microfluidic Device. *PLoS One* **8,** (2013).
34 Yin, L., Wu, Y., Yang, Z., Tee, C. A., Denslin, V., Lai, Z., Lim, C. T., Lee, E. H., & Han, J. Microfluidic label-free selection of mesenchymal stem cell subpopulation during culture expansion extends the chondrogenic potential *in vitro*. *Lab Chip* **18,** 878–889 (2018).
35 Poon, Z., Lee, W. C., Guan, G., Nyan, L. M., Lim, C. T., Han, J., Vliet, K. J. Van, & Van Vliet, K. J. Bone Marrow Regeneration Promoted by Biophysically Sorted Osteoprogenitors From Mesenchymal Stromal Cells. *Stem Cells Transl. Med.* **4,** 56–65 (2015).
View Article Online DOI: 10.1039/C8LC01154K
36 McGrath, J., Jimenez, M., & Bridle, H. Deterministic lateral displacement for particle separation: a review. *Lab Chip* **14,** 4139–58 (2014).
37 Huang, L. R., Cox, E. C., Austin, R. H., & Sturm, J. C. Continuous Particle Separation Through Deterministic Lateral Displacement. *Science (80-.).* **304,** 987–990 (2004).
38 Beech, J. P., Holm, S. H., Adolfsson, K., & Tegenfeldt, J. O. Sorting cells by size, shape and deformability. *Lab Chip* **12,** 1048 (2012).
39 Beech, J. P., Ho, B. D., Garriss, G., Oliveira, V., Henriques-Normark, B., & Tegenfeldt, J. O. Separation of pathogenic bacteria by chain length. *Anal. Chim. Acta* **1000,** 223–231 (2018).
40 Holmes, D., Whyte, G., Bailey, J., Vergara-Irigaray, N., Ekpenyong, A., Guck, J., & Duke, T. Separation of blood cells with differing deformability using deterministic lateral displacement. *Interface Focus* **4,** 20140011 (2014).
41 Davis, J. a, Inglis, D. W., Morton, K. J., Lawrence, D. a, Huang, L. R., Chou, S. Y., Sturm, J. C., & Austin, R. H. Deterministic hydrodynamics: taking blood apart. *Proc. Natl. Acad. Sci. U. S. A.* **103,** 14779–14784 (2006).
42 Holm, S. H., Beech, J. P., & Tegenfeldt, J. O. Combined Density and Size-based Sorting in Deterministic Lateral Displacement Devices. in *17th International Conference on Miniaturized Systems for Chemistry and Life Sciences* 1224–1226 (2013).
43 Collins, D. J., Alan, T., & Neild, A. Particle separation using virtual deterministic lateral displacement (vDLD). *Lab Chip* **14,** 1595–603 (2014).
44 Beech, J. P., Jönsson, P., & Tegenfeldt, J. O. Tipping the balance of deterministic lateral displacement devices using dielectrophoresis. *Lab Chip* **9,** 2698–2706 (2009).
45 Xavier, M., Rosendahl, P., Herbig, M., Kräter, M., Spencer, D., Bornhäuser, M., Oreffo, R. O. C., Morgan, H., Guck, J., & Otto, O. Mechanical phenotyping of primary human skeletal stem cells in heterogeneous populations by real-time deformability cytometry. *Integr. Biol. (Camb).* **8,** 616–623 (2016).
46 Jones, E., & McGonagle, D. Human bone marrow mesenchymal stem cells in vivo. *Rheumatology* **47,** 126–131 (2008).
47 Holm, S. H., Beech, J. P., Barrett, M. P., & Tegenfeldt, J. O. Simplifying microfluidic separation devices towards field-detection of blood parasites. *Anal. Methods* **8,** 3291–3300 (2016).
48 Inglis, D. W. Efficient microfluidic particle separation arrays. *Appl. Phys. Lett.* **94,** 013510 (2009).
49 Kierszenbaum, A. L., & Tres, L. L. *Histology and cell biology : an introduction to pathology*.
50 Ovalle, W. K., Nahirney, P. C., & Netter, F. H. (Frank H. *Netter's essential histology*. (Elsevier/Saunders, 2013).
51 Lowe, J. S. (James S., Anderson, P. G. (Pathologist), & Preceded by (work): Stevens, A. (Pathologist). *Stevens & Lowe's human histology*.
52 Tare, R. S., Mitchell, P. D., Kanczler, J., & Oreffo, R. O. C. Bone Research Protocols. **816,** 643 (2012).
53 Williams, E. L., White, K., & Oreffo, R. O. C. Isolation and Enrichment of Stro-1 Immunoselected Mesenchymal Stem Cells from Adult Human Bone Marrow. in *Methods in molecular biology* 67–73 (Humana Press, 2013).
54 Loutherback, K., D'Silva, J., Liu, L., Wu, A., Austin, R. H., & Sturm, J. C. Deterministic separation of cancer cells from blood at 10 mL/min. *AIP Adv.* **2,** 0–7 (2012).
55 Hur, S. C., Henderson-MacLennan, N. K., McCabe, E. R. B., & Di Carlo, D. Deformability-based cell classification and enrichment using inertial microfluidics. *Lab Chip* **11,** 912–920 (2011).

Lab on a Chip ARTICLE

56 Fachin, F., Spuhler, P., Martel-Foley, J. M. *et al.* Monolithic Chip for High- throughput Blood Cell Depletion to Sort Rare Circulating Tumor Cells. *Sci. Rep.* **7,** 10936 (2017).

View Article Online
DOI: 10.1039/C8LC01154K